frontiers | Frontiers in Marine Science

ORIGINAL RESEARCH
published: 04 May 2022
doi: 10.3389/fmars.2022.884951

# Porewater-Derived Blue Carbon Outwelling and Greenhouse Gas Emissions in a Subtropical Multi-Species Saltmarsh

*Peiyuan Zhu[1†], Xiaogang Chen[1,2*†], Yan Zhang[1†], Qianyu Zhang[3†], Xuan Wu[1], Huawen Zhao[1], Liang Qi[1†], Xuexin Shao[4†] and Ling Li[1*†]*

[1] Key Laboratory of Coastal Environment and Resources of Zhejiang Province, School of Engineering, Westlake University, Hangzhou, China, [2] Insititute of Advanced Technology, Westlake Institute for Advanced Study, Hangzhou, China, [3] Department of Civil and Environmental Engineering, Washington State University, Pullman, WA, United States, [4] Wetland Ecosystem Research Station of Hangzhou Bay, Research Institute of Subtropical Forestry, Chinese Academy of Forestry, Hangzhou, China

Saltmarshes can sequester atmospheric $CO_2$ in sediments, but limited studies have quantified porewater-derived carbon exports and identified related carbon sources. Here, we estimated porewater exchange, carbon outwelling, and greenhouse gas emissions in a subtropical multi-species saltmarsh. The radon-based porewater exchange rate was estimated to be 5.60 ± 2.78 cm $d^{-1}$. As the most dominant (~90%) carbon species, dissolved inorganic carbon (DIC) fluxes through porewater exchange and outwelling were 447 ± 227 and 1200 ± 61 mmol $m^{-2}$ $d^{-1}$, respectively, which were 1.2 and 3.2 times that of carbon burial. As most DIC can remain in the ocean for a long time, porewater-derived DIC outwelling represents another important carbon sink, in addition to carbon burial. $CO_2$ and $CH_4$ emissions from creek water were 54.6 ± 0.5 and 0.19 ± 0.01 mmol $m^{-2}$ $d^{-1}$, respectively, which could offset 16% of carbon burial. The $\delta^{13}C$ and C/N ratios suggest that saltmarsh organic carbon mainly originates from the C3 plant *Scirpus mariqueter* rather than the C4 plant *Spartina alterniflora*. Overall, we suggest that porewater-derived DIC outwelling is an important long-term carbon sink in multi-species saltmarshes, providing a scientific basis for the protection and restoration of saltmarshes in the context of global climate change.

**Keywords: saltmarsh biodiversity, carbon sequestration, coastal blue carbon, lateral carbon exports, carbon budget, C3 and C4 plant species, carbon isotope $\delta^{13}C$, Hangzhou Bay**

OPEN ACCESS

***Edited by:***
*Kai Xiao,*
*Southern University of Science and Technology, China*

***Reviewed by:***
*Ding He,*
*Hong Kong University of Science and Technology, Hong Kong SAR, China*
*Qiugui Wang,*
*Guangzhou University, China*
*Bochao Xu,*
*Ocean University of China, China*

****Correspondence:***
*Xiaogang Chen*
*chenxiaogang@westlake.edu.cn*
*Ling Li*
*liling@westlake.edu.cn*

***†ORCID:***
*Peiyuan Zhu*
*orcid.org/0000-0003-2996-6629*
*Xiaogang Chen*
*orcid.org/0000-0003-4329-0530*
*Yan Zhang*
*orcid.org/0000-0002-8874-6709*
*Qianyu Zhang*
*orcid.org/0000-0002-5316-0767*
*Liang Qi*
*orcid.org/0000-0002-1874-648X*
*Xuexin Shao*
*orcid.org/0000-0002-3214-6085*
*Ling Li*
*orcid.org/0000-0001-8725-1221*

***Specialty section:***
*This article was submitted to Marine Ecosystem Ecology, a section of the journal Frontiers in Marine Science*

***Received:*** *27 February 2022*
***Accepted:*** *04 April 2022*
***Published:*** *04 May 2022*

## 1 INTRODUCTION

Vegetated saltmarshes are crucial coastal blue carbon ecosystems with high carbon stocks and sequestration (McLeod et al., 2011). Atmospheric $CO_2$ photosynthetically sequestered via saltmarsh vegetation can be stored in biomass and then buried in sediments (Duarte et al., 2005; Lo Iacono et al., 2008). Although saltmarshes and other coastal wetlands, such as mangroves and seagrasses, cover only 0.2% of the global ocean surface, 50% of the carbon burial in ocean sediments originates

from these coastal wetlands (Duarte et al., 2013). While saltmarshes are considered an important carbon sink, sediment carbon would potentially release from soil (Herrmann et al., 2015; Najjar et al., 2018). Microorganisms can cause decomposition of some sediment carbon into greenhouse gases (e.g., $CO_2$ and $CH_4$) and organic/inorganic carbon matter (Tang et al., 2018; Chen et al., 2020b). Then, these decomposed carbon species can be partially released into the adjacent ocean through porewater exchange (Santos et al., 2019; Liu et al., 2021; Tamborski et al., 2021; Chen et al., 2022; He et al., 2022). Globally, considerable amounts of carbon were transported into coastal waters through mangrove groundwater flow, which accounts for 29–48% of global riverine export to the ocean (Chen et al., 2018). However, limited studies focus on porewater-derived carbon exports and greenhouse gas emissions in saltmarsh ecosystems.

The flow of water through continental and insular margins, from the seabed to the coastal ocean, was defined as submarine groundwater discharge (Taniguchi et al., 2019). In saltmarshes, submarine groundwater discharge mainly relates to processes with sub-meter length scale (i.e., tidal and wave pumping, shear flow, and ripple migration), which can be more specific to porewater exchange (Taniguchi et al., 2019; Garcia-Orellana et al., 2021). As the surface water-groundwater exchange in coastal wetlands is mainly seawater circulation rather than fresh groundwater discharge, to emphasize the seawater circulation process in the root zone of coastal wetlands, the surface water-groundwater exchange is usually expressed by porewater exchange (e.g., Tait et al., 2016; Santos et al., 2019; Chen et al., 2021b; Chen et al., 2022; Wang et al., 2022). The interaction between porewater/groundwater and surface water is significantly affected by bioturbations, such as crab burrows (Xin et al., 2009; Xiao et al., 2020; Santos et al., 2021b; Xin et al., 2022). Quantifying the porewater exchange rate is essential to determine the transportation of carbon species across the sediment-water interface. Radon ($^{222}$Rn) is a useful natural radioisotope for quantifying carbon exports associated with porewater exchange by integrating $^{222}$Rn fluxes that occur within a broad area of influence (Correa et al., 2021). $^{222}$Rn has been employed to estimate porewater exchange rates and related carbon fluxes in mangroves (Chen et al., 2018; Taillardat et al., 2018; Chen et al., 2021a; Wu et al., 2021) and saltmarshes (Chen et al., 2021b; Correa et al., 2021; Liu et al., 2021).

Carbon burial rates in saltmarshes have been quantified 1–3 orders of magnitude higher than those in terrestrial forests (McLeod et al., 2011; Duarte et al., 2013). Saltmarshes provide habitats for a diversity of salt- and/or saturation-tolerant plant species with high productivity (Guimond and Tamborski, 2021). However, plant biomass varies with species; thus, succession and invasion of saltmarsh vegetation can directly affect carbon composition and content in sediments (Seyfferth et al., 2020). In 1979, *Spartina alterniflora*, originally North America, was introduced into China for sediment accumulation due to strong root systems (Gao et al., 2012) and then rapidly spread in the eastern Chinese coastal region (Gao et al., 2014). Previous studies have found that sediment carbon burial rates change with different vegetation cover, such as *Scirpus mariqueter* and *Spartina alterniflora* (Xia et al., 2019). However, the mechanism and extent of porewater-derived carbon outwelling and greenhouse gas emissions in multi-species saltmarshes remain unknown.

Here, we hypothesized that porewater exchange is the major driving force of carbon outwelling and greenhouse gas emissions in multi-species salt marshes. We investigated spatial $^{222}$Rn, carbon (dissolved inorganic carbon (DIC) and dissolved organic carbon (DOC)), and greenhouse gas ($CO_2$ and $CH_4$) distributions for both intertidal porewater and surface water in a subtropical multi-species saltmarsh (Andong Shoal, China). In addition, we analyzed the contents of organic carbon, nitrogen, and $\delta^{13}$C isotopes in different saltmarsh vegetation. The objectives of this study were to (1) trace the origin of organic carbon in saltmarsh sediments, surface water, and porewater using the $\delta^{13}$C carbon isotope signature; (2) quantify the porewater exchange rate using a $^{222}$Rn mass balance model; and (3) estimate the fluxes of porewater-derived carbon outwelling and greenhouse gas emissions.

# 2 MATERIALS AND METHODS

## 2.1 Study Region

Field investigations were performed in a multi-species saltmarsh, Andong Shoal, located on the protruding section of the tidal shoal on the south bank of Hangzhou Bay, China (**Figure 1**). Andong Shoal is an alluvial coast and has a subtropical monsoon climate with a mean annual temperature of 17.1°C and mean annual rainfall of 1381 mm (Cao et al., 2020). It is formed by the accumulation of sediments from the Yangtze and Qiantang River (Wu et al., 2008). The intertidal zone of Andong Shoal is 7–8 km wide (Song et al., 2014), with a developed creek system due to macrotidal conditions (Li and Xie, 1993). An irregular semidiurnal tide exists in this region, with a mean tidal range of 5.5 m (Huang et al., 2020). The vegetation in the saltmarsh includes not only local species such as *Scirpus mariqueter*, *Suaeda glauca*, and *Phragmites australis* (C3 plant species), but also invasive species such as *Spartina alterniflora* (C4 plant species) (Wang et al., 2015).

## 2.2 Sampling and Analytical Methods

### 2.2.1 Surface Water and Porewater

Field work was performed in saltmarsh tidal creeks along the Andong Shoal (**Figure 1**) during the wet season (May 2021) due to its obvious porewater flow (Young et al., 2005; Chen et al., 2018). Surface water samples (n=36) were directly pumped into 2 L polyethylene bottles using the overflow method (Chen et al., 2018). Then, the sampling bottle was connected in a close air loop with a RAD-7 detector (Durridge) and a Picarro G4301 for measuring $^{222}$Rn and greenhouse gases (including $CO_2$ and $CH_4$), respectively (Santos et al., 2012). In addition, each water sample was filtered through 0.45-μm nylon filters into 60 mL polyethylene bottles without headspace, in triplicate for DIC/DOC, organic nitrogen, and stable carbon isotope ($\delta^{13}$C)

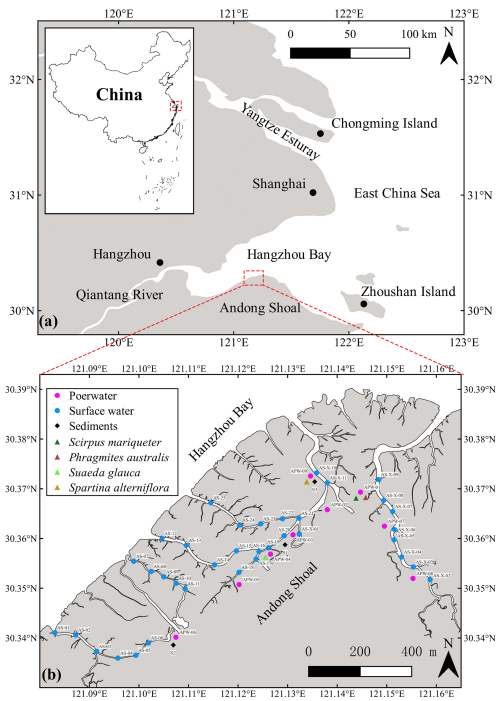


**FIGURE 1** | **(A)** Location of the study area (Andong Shoal); **(B)** Sampling stations for creek surface water, sediments and vegetations.

measurements. These filtrates were preserved by a saturated $HgCl_2$ solution (Gatland et al., 2014; Santos et al., 2019), which can eliminate the influence on the amount of carbon species *via* the microorganism process. Surface water temperature, salinity, water depth, pH, and dissolved oxygen (DO) profiles were recorded using an EXO3 Multiparameter Sonde automated datalogger. Wind speed data was obtained from the China Meteorological Data Service Center (http://data.cma.cn/). To approach the $^{222}$Rn ingrowth from $^{226}$Ra, surface waters were slowly passed through $MnO_2$-impregnated acrylic fibers for $^{226}$Ra enrichment, and the fibers were then washed with Milli-Q water to remove slats and particles (Moore and Arnold, 1996). These $^{226}$Ra-enrichment fibers were sealed for three months and subsequently analyzed using a RAD-7 detector (Peterson et al., 2009).

Porewater bores (n=9) were installed along the saltmarsh creek to capture the spatial variability in the Andong Shole (**Figure 1**). Samples of porewater $^{222}$Rn, $CO_2$, and $CH_4$ were collected in 2-L polyethylene bottles and analyzed using the same methods as the surface water. The DIC/DOC, organic nitrogen, and $\delta^{13}$C samples were collected and treated as described earlier. In addition, the porewater temperature, salinity, pH, and DO were measured using a Multi 3430 WTW digital multi-parameter meter.

DIC and DOC samples of the surface water and porewater were analyzed using a TOC-L (Shimadzu, Japan) total organic carbon analyzer (Chen et al., 2018). DIC concentrations were directly measured by injecting water samples into the reactor with spiked hydrochloric acid. DOC concentrations were considered as the difference between the total dissolved carbon (TDC) and DIC. To determine the TDC concentrations, water samples were combusted in a 680°C tube with a catalyst. The measurement errors were ±4% for DIC and ±5% for TDC, with a precision of < ± 1%. Organic nitrogen represents the difference between total nitrogen and dissolved inorganic nitrogen (including $NO_3$-N, $NO_2$-N, $NH_4$-N). The concentrations of total nitrogen and dissolved inorganic nitrogen were measured using a San$^{++}$ continuous flow analyzer by adapting spectrophotometric method (Kroon, 1993; Liu et al., 2009). Organic $^{13}$C isotope samples were analyzed using an ISOPRIME100 (Elementar, Germany) stable isotope mass ratio spectrometer and calculated as $\delta^{13}$C values referring to the international standard Vienna Pee Dee Belemnite (VPDB) (Degens, 1969). Replicate analysis of the laboratory standard samples indicated a precision of ±0.16%.

### 2.2.2 Sediments and Saltmarsh Plants

Saltmarsh sediment samples were collected to estimate $^{222}$Rn diffusive flux using a sediment equilibration experiment (Corbett et al., 1998). One liter or 1.5 kg of sediment was incubated with 5 L of radium-free water in a sealed flask for three months. Once the dissolved $^{222}$Rn had equilibrated between water and sediment, 2 L of water was pumped into a polyethylene bottle, and the $^{222}$Rn concentration was analyzed using a RAD-7 detector. Sediment cores and saltmarsh plant samples, such as *Scirpus mariqueter*, *Spartina alterniflora*, *Suaeda glauca*, and *Phragmites australis*, were collected (**Figure 1**). The sediment samples were sealed in aluminum foil bags and stored at -40°C. For saltmarsh plants, each species was cleaned, separated into leaves, stems, and roots, and then stored using the same method as the sediment samples. Sediment and plant samples were analyzed for organic carbon, organic nitrogen, and $\delta^{13}$C values using a 253plus (Thermo Scientific, US) isotope ratio mass spectrometer (Pérez et al., 2020). The $\delta^{13}$C values were calculated by referring to the VPDB. The precisions were ±0.5% for organic carbon, ± 1% for organic nitrogen and ±0.05% for $\delta^{13}$C.

## 2.3 $^{222}$Rn Mass Balance Model, Carbon Outwelling and Greenhouse Gas Emissions

The $^{222}$Rn mass balance model (Burnett and Dulaiova, 2003) has been widely used to quantify advective porewater flux in saltmarshes and mangroves (e.g., Santos et al., 2019; Correa et al., 2021; Chen et al., 2022). The model integrates all $^{222}$Rn sources (e.g., imports from bay water during the flood tide, diffusion from sediments, and ingrowth from dissolved $^{226}$Ra) and sinks (exports during the ebb tide, atmospheric evasion, and radioactive decay). Surface water samples were collected during the highest tide level, because the sampling boat can reach the upstream sites at this time. Assuming all the creek water is

discharged during ebb tide, the missing $^{222}$Rn represents porewater exchange in each tidal cycle. At steady state, integrating all of fluxes over a complete day, the porewater exchange flux ($F_{pw}$, Bq m$^{-2}$ d$^{-1}$) can be estimated as follows:

$$F_{pw} = \frac{(^{222}Rn_{sw} \cdot \Delta V) + F_{atm} + (\lambda \times \Delta V \times {}^{222}Rn_{sw}) - (^{222}Rn_{sea} \cdot \Delta V) - F_{sed} - (\lambda \times \Delta V \times {}^{226}Ra_{sw})}{A} \quad (1)$$

where $^{222}Rn_{sw}$ is the average $^{222}$Rn activity (Bq m$^{-3}$) in surface water during the flood tide, $\Delta v$ is the difference of water volume in creeks between high tide level and low tide level (m$^3$ d$^{-1}$), $F_{atm}$ is the $^{222}$Rn flux to the atmosphere (Bq m$^{-2}$ d$^{-1}$), which can be calculated by concentration gradients, wind speed and current (Chen et al., 2020a), $\lambda$ is the $^{222}$Rn decay constant (0.182 d$^{-1}$), $^{222}Rn_{sea}$ is the $^{222}$Rn activity (Bq m$^{-3}$) of seawater end-member, $F_{sea}$ is the $^{222}$Rn flux *via* sediment diffusion (Bq m$^{-2}$ d$^{-1}$), $^{226}Ra_{sw}$ is the $^{226}$Ra concentration in surface water, and $A$ is the inundated area (m$^2$).

Similar to the $^{222}$Rn calculation, carbon outwelling ($F_{outwelling}$, mmol m$^{-2}$ d$^{-1}$) from intertidal creeks was estimated as follows:

$$F_{outwelling} = \frac{(C_{sw} - C_{sea}) \times \Delta V}{A} \quad (2)$$

where $C_{sw}$ is the concentration of carbon species in surface water (mmol L$^{-1}$) and $C_{sea}$ is the corresponding seawater endmember of the carbon species (mmol L$^{-1}$).

Greenhouse gas emissions at the water-air interface were calculated from a bulk flux equation (Wanninkhof, 2014); therefore, greenhouse gas emissions ($F_{emissions}$, mmol m$^{-2}$ d$^{-1}$), including $CO_2$ and $CH_4$, from creek water were estimated as follows:

$$F_{emissions} = k\alpha(C_{sw} - C_{air}) \quad (3)$$

where $C_{sw}$ is the greenhouse gas concentration in surface water (mmol L$^{-1}$), $C_{air}$ is the greenhouse gas concentration in air (mmol L$^{-1}$), and $k$ is the gas transfer velocity (m d$^{-1}$), which was the mean value derived from three gas transfer models (Borges et al., 2004; Ho et al., 2016; Rosentreter et al., 2017), $\alpha$ is the solubility coefficient of greenhouse gas. Uncertainties regarding the $^{222}$Rn mass balance model and carbon fluxes are estimated based on the basic rules of error propagation.

# 3 RESULTS AND DISCUSSION

## 3.1 Surface Water and Porewater Observations

During the surface water observation, temperature and salinity were found with spatial gradients, whereas DO and pH were

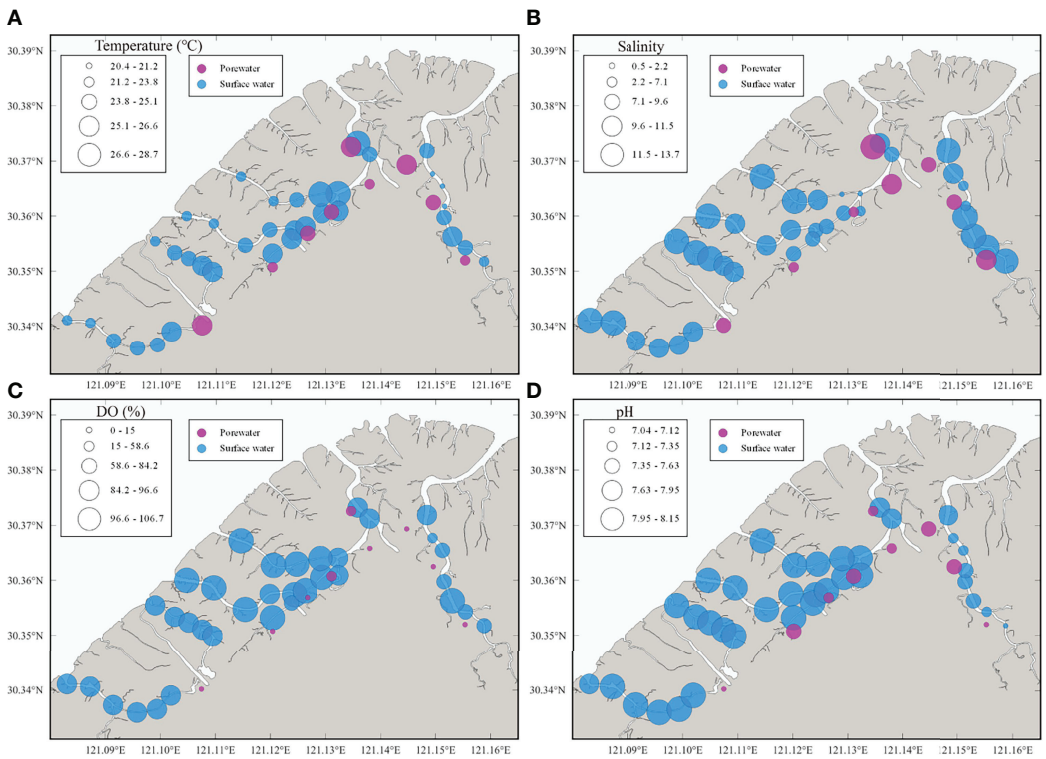


**FIGURE 2** | Spatial distributions of **(A)** temperature, **(B)** salinity, **(C)** DO and **(D)** pH in surface water and porewater.

**TABLE 1** | Summary of surface water observations.

| Sample ID | Temperature °C | Salinity | DO % (mg $L^{-1}$) | pH | Radon Bq $m^{-3}$ | $CO_2$ μmol $L^{-1}$ | $CH_4$ nmol $L^{-1}$ | DIC mmol $L^{-1}$ | DOC mmol $L^{-1}$ |
|---|---|---|---|---|---|---|---|---|---|
| AS-01 | 23.8 | 12.7 | 94.4 (8.00) | 7.95 | 31 ± 10 | 30 | 139 | 1.78 | 0.41 |
| AS-02 | 23.5 | 12.5 | 94.7 (8.01) | 8.04 | 10 ± 6 | 35 | 161 | 1.74 | 0.37 |
| AS-03 | 24.7 | 11.5 | 95 (7.88) | 8.05 | 41 ± 14 | 30 | 208 | 1.81 | 0.32 |
| AS-04 | 25.1 | 11.1 | 96.1 (7.87) | 8.07 | 26 ± 11 | 35 | 257 | 1.81 | 0.32 |
| AS-05 | 25.1 | 10.7 | 94.7 (7.76) | 8.07 | 25 ± 12 | 31 | 233 | 1.69 | 0.35 |
| AS-06 | 25.7 | 10.2 | 96.6 (7.85) | 8.09 | 26 ± 12 | 36 | 216 | 1.69 | 0.50 |
| AS-07 | 23.6 | 13.2 | 95.1 (8.02) | 8.12 | 32 ± 13 | 33 | 165 | 1.74 | 0.45 |
| AS-08 | 24.2 | 12.4 | 95.1 (7.93) | 8.12 | 46 ± 16 | 37 | 189 | 1.73 | 0.40 |
| AS-09 | 24.6 | 11.7 | 95.3 (7.88) | 8.11 | 21 ± 11 | 30 | 189 | 1.81 | 0.30 |
| AS-10 | 25.5 | 11.1 | 95.2 (7.75) | 8.09 | 36 ± 17 | 37 | 295 | 1.93 | 0.23 |
| AS-11 | 26.6 | 10.6 | 94.6 (7.54) | 8.05 | 47 ± 18 | 46 | 291 | 2.14 | 0.45 |
| AS-12 | 23.1 | 12.0 | 99.8 (8.00) | 8.15 | 32 ± 13 | 35 | 182 | 1.71 | 0.36 |
| AS-13 | 23.5 | 11.0 | 99.1 (7.90) | 8.14 | 15 ± 8 | 33 | 180 | 1.70 | 0.46 |
| AS-14 | 24.0 | 11.0 | 98.7 (7.84) | 8.11 | 19 ± 9 | 37 | 201 | 1.69 | 0.47 |
| AS-15 | 24.5 | 10.3 | 95.3 (7.56) | 8.08 | 40 ± 14 | 33 | 189 | 1.68 | 0.44 |
| AS-16 | 25.4 | 9.0 | 99.8 (7.79) | 8.10 | 19 ± 9 | 34 | 189 | 1.68 | 0.36 |
| AS-17 | 25.8 | 9.1 | 71.1 (5.53) | 8.09 | 20 ± 10 | 29 | 176 | 1.61 | 0.52 |
| AS-18 | 26.5 | 8.6 | 105 (8.06) | 8.13 | 23 ± 11 | 29 | 115 | 1.69 | 0.35 |
| AS-19 | 25.6 | 9.3 | 100.9 (7.84) | 8.10 | 44 ± 17 | 35 | 209 | 1.66 | 0.33 |
| AS-20 | 26.0 | 9.2 | 103 (7.95) | 8.12 | 27 ± 11 | 32 | 183 | 1.64 | 0.34 |
| AS-21 | 27.4 | 0.5 | 92.7 (7.08) | 8.03 | 96 ± 25 | 49 | 161 | 1.54 | 0.57 |
| AS-22 | 27.1 | 2.2 | 101.5 (7.67) | 8.12 | 105 ± 26 | 45 | 137 | 1.96 | 0.55 |
| AS-23 | 24.9 | 11.1 | 101.7 (7.91) | 8.15 | 28 ± 12 | 34 | 200 | 1.71 | 0.35 |
| AS-24 | 23.3 | 12.5 | 100.3 (7.98) | 8.15 | 23 ± 10 | 44 | 249 | 1.74 | 0.33 |
| AS-25 | 23.1 | 12.9 | 101.6 (8.08) | 8.11 | 32 ± 15 | 35 | 173 | 1.75 | 0.30 |
| AS-X-01 | 25.4 | 4.5 | 91.5 (7.52) | 8.08 | 521 ± 64 | 105 | 939 | 5.01 | 0.75 |
| AS-X-02 | 22.3 | 12.0 | 78.3 (6.81) | 7.11 | 94 ± 23 | 71 | 313 | 2.52 | 0.51 |
| AS-X-03 | 24.1 | 12.0 | 82.7 (6.94) | 7.35 | 122 ± 27 | 70 | 248 | 2.66 | 0.58 |
| AS-X-04 | 26.4 | 13.7 | 106.7 (8.61) | 7.42 | 98 ± 25 | 34 | 94 | 1.98 | 0.39 |
| AS-X-05 | 24.9 | 12.4 | 84.2 (6.98) | 7.63 | 144 ± 30 | 92 | 442 | 3.11 | 0.60 |
| AS-X-06 | 20.4 | 5.8 | – | 7.48 | 114 ± 26 | 92 | 346 | 2.97 | 0.79 |
| AS-X-07 | 20.5 | 6.2 | 83.2 (7.46) | 7.19 | 82 ± 22 | 82 | 273 | 2.62 | 0.67 |
| AS-X-08 | 21.2 | 10.9 | 53.6 (4.71) | 7.21 | 325 ± 50 | 179 | 236 | 2.38 | 0.29 |
| AS-X-09 | 24.1 | 11.8 | 92.5 (7.79) | 7.91 | 238 ± 10 | – | – | 6.55 | 0.63 |
| AS-X-10 | 28.7 | 10.6 | 95.2 (7.49) | 7.92 | 249 ± 47 | – | – | 7.90 | 0.70 |
| AS-X-11 | 24.7 | 9.0 | 93.9 (7.76) | 7.82 | 51 ± 17 | 110 | 195 | 1.84 | 0.31 |

relatively stable (**Figure 2** and **Table 1**). The surface water temperature increased from downstream (20.4°C) to upstream (28.7°C) while the salinity showed a contrasting trend decreasing from 13.7 to 0.5. Surface water DO and pH were irregularly distributed in ranges of 54–107% (4.7–8.6 mg $L^{-1}$) (mean: 94 ± 10%, 7.6 ± 0.7 mg $L^{-1}$) and 7.1–8.2 (mean: 7.9 ± 0.3), respectively, and the lowest pH were measured at upstream of creeks. $^{222}$Rn, carbon, and greenhouse gases showed large spatial heterogeneity, indicating the necessity for spatial investigation (**Figure 3**). Surface water parameters varied over a range of 10–521 (mean: 81 ± 103) Bq $m^{-3}$ for $^{222}$Rn, 1.54–7.90 (mean: 2.31 ± 1.36) mmol $L^{-1}$ for DIC, 0.23–0.79 (mean: 0.45 ± 0.14) mmol $L^{-1}$ for DOC, 29–179 (mean: 51 ± 32) μmol $L^{-1}$ for $CO_2$ and 94–939 (mean: 235 ± 140) nmol $L^{-1}$ for $CH_4$. Carbon species in surface water were dominated by DIC with various DOC proportions (12%–26%) and negligible greenhouse gases (**Figure 4**).

All hydrological parameters in porewater samples showed spatial heterogeneity (**Figures 2**, **3** and **Table 2**). Temperature, salinity, DO and pH changed from 22.6 to 26.3°C, 4.7 to 11.7, 0.5 to 58.6% (0.03 to 4.73 mg $L^{-1}$) and 7.04 to 7.54, with mean values of 24.6 ± 1.2°C, 8.71 ± 2.46, 13.8 ± 19.3% (1.2 ± 1.5 mg $L^{-1}$) and 7.32 ± 0.16, respectively. Porewater $^{222}$Rn activities varied from $1.01\times10^3$ Bq $m^{-3}$ to $4.91\times10^3$ Bq $m^{-3}$ with the mean value of $(1.95 \pm 2.02)\times10^3$ Bq $m^{-3}$, which was approximately 24-fold higher than that in surface water. Carbon and greenhouse gases displayed considerable variability in porewater. As expected, DIC (range: 5.6–15.4 mmol $L^{-1}$, mean: 10.1 ± 3.0 mmol $L^{-1}$), DOC (range: 0.28–1.78 mmol $L^{-1}$, mean: 0.85 ± 0.41 mmol $L^{-1}$), $CO_2$ (range: 325–1280 μmol $L^{-1}$, mean: 709 ± 277 μmol $L^{-1}$) and $CH_4$ (range: 551–138400 nmol $L^{-1}$, mean: 6580 ± 4510 nmol $L^{-1}$) were highly enriched in porewater, which were approximately 4.5, 1.9, 14.2 and 28.1 times their respective concentrations in surface water. Similarly, in porewater, the major carbon species was also DIC, while DOC and greenhouse gases were minor components (**Figure 4**). This is because sulfate reduction coupled to pyrite formation effectively convert sediment organic carbon into bicarbonate (the main component of DIC) (Reithmaier et al., 2021).

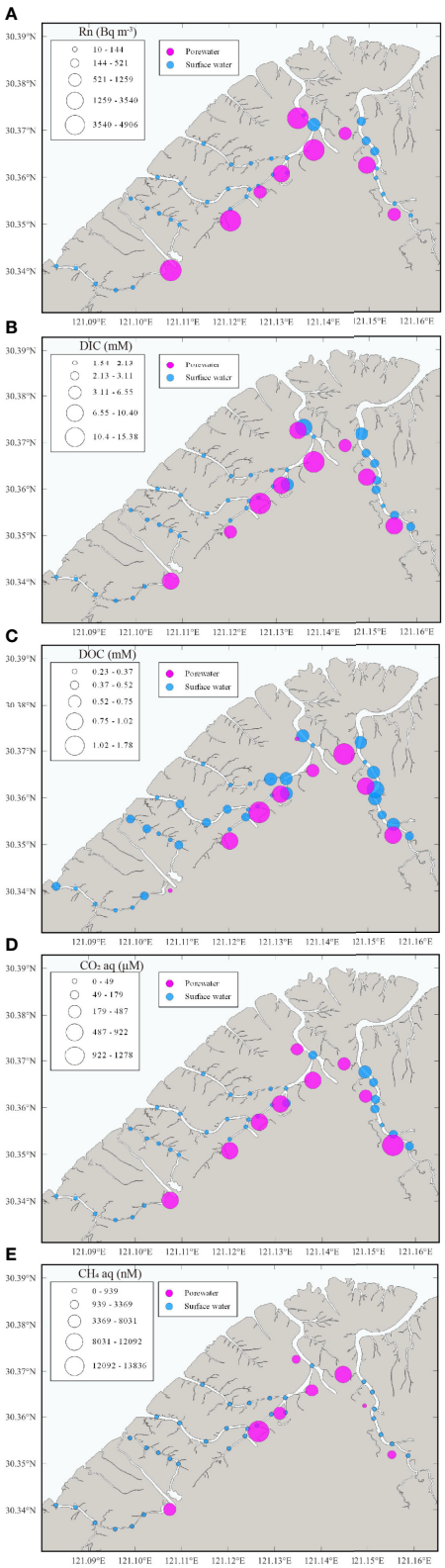


**FIGURE 3** | Spatial distributions of **(A)** $^{222}$Rn, **(B)** DIC, **(C)** DOC, **(D)** CO2 and **(E)** $CH_4$ in surface water and porewater.

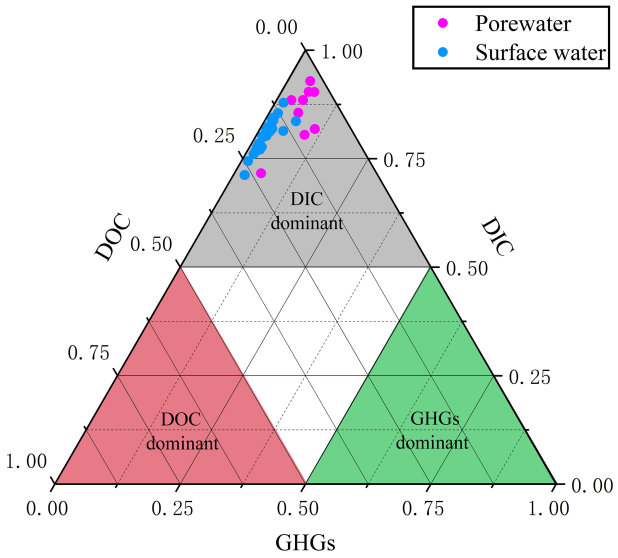


**FIGURE 4** | Ternary diagram illustrating the percentage of different carbon species [DIC, DOC and greenhouse gases (GHGs)] in surface water and porewater.

## 3.2 Source Identification of Organic Carbon in Sediments and Porewater

According to different photosynthetic processes, plants can be divided into C3 and C4 plants, with distinct differences in the proportion of $^{13}$C isotopes. Generally, the $\delta^{13}$C values of C3 plants (range from -34‰ to -23‰) were more negative than those of C4 plants (range from -17‰ to -9‰) (Chmura and Aharon, 1995). In the Andong Shoal, local saltmarsh species, *Scirpus mariqueter*, *Suaeda glauca*, and *Phragmites australis*, were typical C3 plants with $\delta^{13}$C in range from -29‰ to -27‰, but the C4 plant *Spartina alterniflora* had a much higher $\delta^{13}$C of approximately -14‰ (**Table 3** and **Figure 5**). For each plant species, $\delta^{13}$C values were relatively constant for various C/N ratios in the different organs (**Figure 5**).

Combining organic $\delta^{13}$C values with C/N ratios in sediments and porewater can trace the source of organic carbon (Meyers, 1994). In sediment samples, results of $\delta^{13}$C (range from -25.0‰ to -23.8‰) and C/N ratio (range from 9.79 to 11.42) implied that the C3 plant *Scirpus mariqueter* was the major source of sediment organic carbon (**Figure 5** and **Tables 3**, **4**). A low C/N ratio (<10) may indicate that organic carbon was provided by lake or marine algae (Meyers, 1994). While lake algae would not be the source of organic carbon as no direct connection with lake ecosystems, marine algae can be a potential source because of frequent algal blooms around Hangzhou Bay (Liu et al., 2013). Sediment organic carbon was not influenced by the invasion of *Spartina alterniflora*, because of the low density in our study region. Furthermore, in the porewater samples, $\delta^{13}$C values of DOC were relatively constant at -26‰, but C/N ratios varied from 22.28 to 79.48 (**Table 4**). Here, we suggest that porewater-derived DOC flux was mainly provided by the

**TABLE 2 |** Summary of porewater observations.

| Sample ID | Temperature °C | Salinity | DO % (mg $L^{-1}$) | pH | Radon Bq $m^{-3}$ | $CO_2$ µmol $L^{-1}$ | $CH_4$ nmol $L^{-1}$ | DIC mmol $L^{-1}$ | DOC mmol $L^{-1}$ |
|---|---|---|---|---|---|---|---|---|---|
| APW1 | 26.3 | 9.5 | 1.0 (0.07) | 7.54 | 1006 ± 118 | 403 | 11062 | 5.55 | 1.78 |
| APW2 | 23.4 | 10.1 | 0.5 (0.03) | 7.20 | 4906 ± 327 | 922 | 8031 | 15.38 | 0.71 |
| APW3 | 24.9 | 7.1 | 36.6 (3.00) | 7.44 | 2226 ± 146 | 612 | 3369 | 9.12 | 0.92 |
| APW4 | 24.5 | 4.8 | 1.9 (0.14) | 7.34 | 4513 ± 393 | 849 | 12092 | 14.44 | 1.02 |
| APW5 | 23.3 | 4.7 | 1.1 (0.84) | 7.43 | 4474 ± 308 | 750 | 13836 | 6.43 | 0.79 |
| APW6 | 25.5 | 9.4 | 7.6 (0.62) | 7.12 | 3540 ± 175 | 755 | 4552 | 10.40 | 0.35 |
| APW7 | 24.8 | 9.6 | 1.9 (0.14) | 7.49 | 1259 ± 127 | 325 | 551 | 9.73 | 0.94 |
| APW8 | 22.6 | 11.5 | 15.0 (1.30) | 7.04 | 478 ± 202 | 1278 | 2946 | 9.55 | 0.84 |
| APW9 | 25.8 | 11.7 | 58.6 (4.73) | 7.27 | 1217 ± 99 | 487 | 282 | 10.05 | 0.28 |

**TABLE 3 |** C/N molar ratio and $\delta^{13}C$ value of vegetations in Andong Shoal.

| Vegetations | Root | | Stem | | Leaf | |
|---|---|---|---|---|---|---|
| | C/N | $\delta^{13}C$ (‰) | C/N | $\delta^{13}C$ (‰) | C/N | $\delta^{13}C$ (‰) |
| *Scirpus mariqueter* | 18.10 | -27.50 | 42.29 | -27.42 | 23.60 | -28.37 |
| *Spartina alterniflora* | 98.81 | -13.88 | 22.06 | -13.46 | 52.37 | -13.80 |
| *Suaeda glauca* | 42.33 | -29.34 | 31.23 | -29.33 | 15.23 | -29.37 |
| *Phragmites australis* | 106.63 | -28.77 | 118.39 | -29.17 | 33.18 | -29.48 |

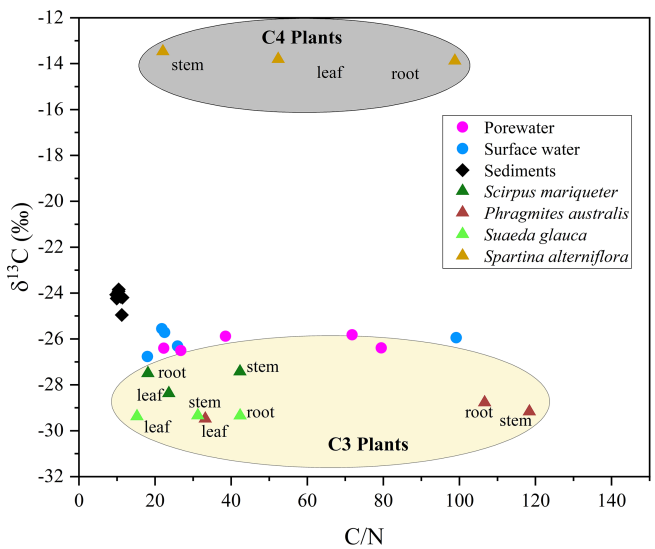


**FIGURE 5 |** Stable carbon isotope of organic carbon in surface water, porewater, sediment and vegetations (including *Scirpus mariqueter*, *Spartina alterniflora*, *Suaeda glauca* and *Phragmites australis*), and corresponding C/N molar ratio.

biomass of *Scirpus mariqueter* due to approximate $\delta^{13}C$ value (**Figure 5**).

## 3.3 $^{222}$Rn-Based Porewater Exchange Rate and Associated Carbon and Greenhouse Gas Fluxes

To access the $^{222}$Rn fluxes *via* porewater exchange in the saltmarsh, all $^{222}$Rn sources and sinks were quantified (**Figure 6**). According to the $^{222}$Rn mass balance model (Equation 1), the $^{222}$Rn flux *via* porewater exchange was 196 ± 87 (Bq $m^{-2}$ $d^{-1}$), which accounted for 64% of the total $^{222}$Rn sources. In contrast, $^{222}$Rn fluxes (Bq $m^{-2}$ $d^{-1}$) *via* influx during flood tide, sediment diffusion, and $^{226}$Ra decay accounted for 22%, 13%, and 0.1% of $^{222}$Rn sources, respectively. Similar results of sediment diffusion and $^{226}$Ra decay were found in other coastal wetlands (Santos et al., 2019; Chen et al., 2021a; Chen et al., 2021b; Wu et al., 2021). In terms of the $^{222}$Rn sinks, outflux

**TABLE 4** | C/N molar ratio and $\delta^{13}C$ value in sediment, surface water and porewater samples.

| Sample ID | Description | C/N | $\delta^{13}C$ |
|---|---|---|---|
| S1-1 | Sediment in depth 0-2cm | 9.79 | -24.07 |
| S1-2 | Sediment in depth 42-44cm | 9.91 | -24.23 |
| S1-3 | Sediment in depth 54-56cm | 11.25 | -24.95 |
| S2 | Surface sediment sample | 11.42 | -24.19 |
| S3-1 | Sediment in depth 10-12cm | 10.42 | -23.84 |
| S3-2 | Sediment in depth 26-28cm | 10.94 | -24.15 |
| S3-3 | Sediment in depth 54-56cm | 10.39 | -23.92 |
| AS-01 | Surface water | 17.97 | -26.77 |
| AS-06 | Surface water | 25.91 | -26.31 |
| AS-12 | Surface water | 21.77 | -25.55 |
| AS-15 | Surface water | 22.47 | -25.71 |
| AS-X-10 | Surface water | 99.15 | -25.94 |
| APW-03 | Porewater | 71.82 | -25.82 |
| APW-05 | Porewater | 79.48 | -26.39 |
| APW-06 | Porewater | 26.76 | -26.50 |
| APW-07 | Porewater | 38.52 | -25.88 |
| APW-09 | Porewater | 22.28 | -26.40 |

during the ebb tide, atmospheric evasion, and $^{222}Rn$ decay accounted for 55%, 41%, and 4%, respectively. $^{226}Ra$ decay and $^{222}Rn$ decay were minor components in the $^{222}Rn$ mass balance model and were negligible because of the relatively low percentage of $^{222}Rn$ sources or sinks.

Determining the porewater endmember is the key step in estimating the porewater exchange rate, which has been considered a major source of uncertainty (Moore and Arnold, 1996). As the large spatial variation of natural tracer concentrations in aquifers (Peterson et al., 2009), collecting numbers of representative sample can help deal with uncertainty (Correa et al., 2021). In this study, to reduce the uncertainty caused by porewater endmember, we conducted a spatial investigation of porewater samples (n=9, **Figure 1**). Here, the porewater endmember was defined as the difference between the median porewater concentration and the median concentration of surface water at the creek mouth (Taillardat et al., 2018). Hence, the radon-derived porewater exchange rate was estimated to be 5.60 ± 2.78 cm $d^{-1}$ using $^{222}Rn$ flux *via* porewater exchange divided by the porewater $^{222}Rn$ endmember. This porewater exchange rate is in the range (3.4–12 cm $d^{-1}$) of other saltmarsh studies, as summarized by Liu et al. (2021).

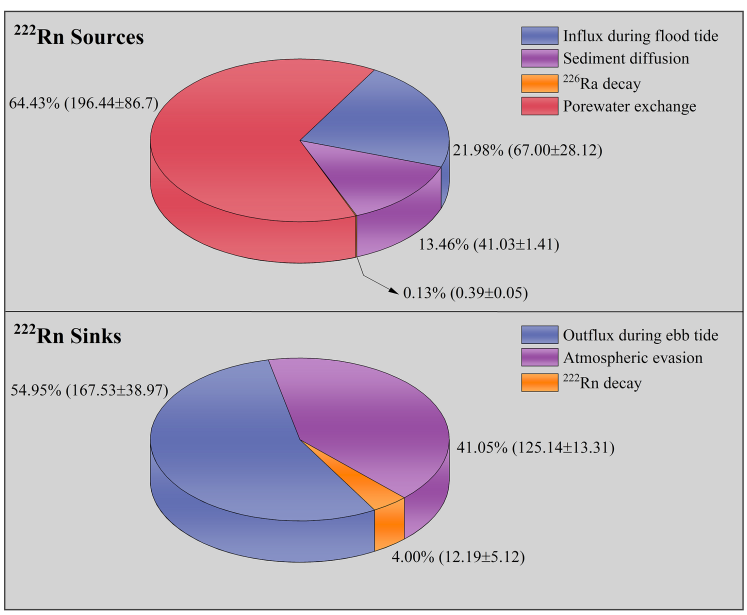


**FIGURE 6** | The $^{222}Rn$ sources and sinks (Bq $m^{-2}$ $d^{-1}$) in Andong Shoal.

Porewater exchange drives the transport of carbon species from the sediment to surface water. This can be proven by the significant positive correlations (**Figure 7**) between $^{222}$Rn and DIC ($R^2$ = 0.49, $p$<0.001), DOC ($R^2$ = 0.27, $p$<0.001), $CO_2$ ($R^2$ = 0.60, $p$<0.001), and $CH_4$ ($R^2$ = 0.62, $p$<0.001) in surface water and higher concentrations of $^{222}$Rn and carbon species in porewater than those in surface water (**Figure 7**). Therefore, we used the difference in median carbon or greenhouse gas values between porewater and surface water as the porewater endmember. By multiplying the porewater exchange rate with the corresponding carbon and greenhouse gas concentrations of porewater endmembers, the porewater-derived carbon and greenhouse gas fluxes (mmol m$^{-2}$ d$^{-1}$) were estimated to be 447 ± 227 (DIC), 26 ± 20 (DOC), 40 ± 21 ($CO_2$), and 0.25 ± 0.13 ($CH_4$) (**Table 5**). Most of the porewater-derived carbon flux was contributed by DIC (~90%) rather than DOC or greenhouse gases. Similar results for DIC, DOC, and $CO_2$ were obtained from a saltmarsh in the USA (Correa et al., 2021). However, porewater-derived carbon flux is mainly sourced from DOC in some other saltmarshes (Santos et al., 2019; Chen et al., 2022). This may be due to their dominant species having higher net primary productivity, leading to the rapid accumulation of organic carbon that can be enriched in porewater (Chen et al., 2022).

## 3.4 Implications of Porewater–Derived Carbon Outwelling and Greenhouse Gas Emissions on Saltmarsh Blue Carbon Budget

### 3.4.1 Carbon Outwelling and Greenhouse Gas Emissions

The outwelling fluxes of DIC, DOC, $CO_2$ and $CH_4$ were estimated to be 1200 ± 61, 115 ± 70, 36.5 ± 0.5, and 0.13 ± 0.01 (mmol m$^{-2}$ d$^{-1}$) (**Table 5**), indicating that tidal creeks were net exporters of DIC, DOC, and greenhouse gases. Carbon outwelling was dominated by DIC (~90%) with minor contributions from DOC and greenhouse gases, providing further evidence that carbon outwelling flux is generally dominated by DIC in saltmarshes (Santos et al., 2021). The DIC outwelling flux (1200 mmol m$^{-2}$ d$^{-1}$) was very close to that of the Chongming Dongtan saltmarsh (Yangtze River Estuary, China) (1050 mmol m$^{-2}$ d$^{-1}$) in the nearby study area investigated by Liu et al. (2021). However, this exceeded the outwelling flux range (9–680 mmol m$^{-2}$ d$^{-1}$) in other study areas (Neubauer and Anderson, 2003; Wang and Cai, 2004; Wang et al., 2016; Chu et al., 2018; Czapla et al., 2020; Chen et al., 2022), which may be due to the macrotidal environment at our study site.

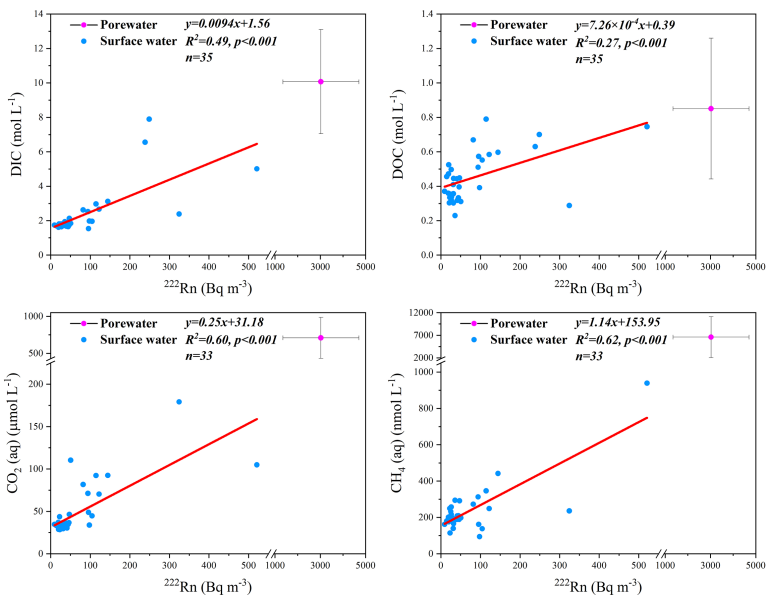


**FIGURE 7** | Correlations of DIC, DOC, $CO_2$ and $CH_4$ with $^{222}$Rn for surface water samples. Porewater samples are included for comparison.

**TABLE 5** | Carbon outwelling and greenhouse gas emissions (mmol m$^{-2}$ d$^{-1}$) in Andong Shoal.

| Carbon species | Porewater exchange | Carbon outwelling | Greenhouse gas emissions |
|---|---|---|---|
| DIC | 447 ± 227 | 1200 ± 61 | – |
| DOC | 26 ± 20 | 115 ± 70 | – |
| $CO_2$ | 40.1 ± 20.7 | 36.5 ± 0.5 | 54.6 ± 0.5 |
| $CH_4$ | 0.25 ± 0.13 | 0.13 ± 0.01 | 0.19 ± 0.01 |

$CO_2$ and $CH_4$ emission fluxes through the water-air interface were estimated to be 54.63 ± 0.45 and 0.19 ± 0.01 (mmol $m^{-2}$ $d^{-1}$) (**Table 5**), implying that tidal creeks of saltmarsh are greenhouse gas sources for atmosphere. The $CO_2$ emission flux (54 mmol $m^{-2}$ $d^{-1}$) was within the emission flux range (2–288 mmol $m^{-2}$ $d^{-1}$) reported in previous studies (Neubauer and Anderson, 2003; Wang and Cai, 2004; Chmura et al., 2016; Chen et al., 2022). Meanwhile, the $CH_4$ emission rate (0.19 mmol $m^{-2}$ $d^{-1}$) in our study area (multi-species saltmarsh) was lower than the emission rate range (0.23–1.29 mmol $m^{-2}$ $d^{-1}$) of other saltmarshes covered by *Spartina patens* (Chmura et al., 2016; Chen et al., 2022). Methylamines released by decaying *Spartina alterniflora* (Wang and Lee, 1994) can be converted to $CH_4$ *via* microorganisms (Yuan et al., 2019; Seyfferth et al., 2020) and stored in the sediment.

### 3.4.2 Role of Porewater-Derived Carbon Fluxes

Organic carbon from *in situ* primary production can be buried in sediments because of the accumulation of detritus and roots (Alongi, 2020; Correa et al., 2021). As carbon burial is a function of mitigating climate change (Duarte et al., 2013; Wang et al., 2021), many previous studies relating to saltmarshes have focused on carbon burial rates (Herrmann et al., 2015; Najjar et al., 2018). The carbon burial rate in Andong Shoal was 140 g $m^{-2}$ $yr^{-1}$ (Xia et al., 2019). However, we found that part of the sediment carbon could be flushed out via porewater exchange, which may lead to an important revision of the saltmarsh blue carbon budget.

To approach the contribution of porewater exchange to the saltmarsh blue carbon budget, we constructed a conceptual model of major carbon flows (**Figure 8**). Some of the buried organic carbon can be converted to DIC by sulfate/Fe-oxide reduction (Santos et al., 2019; Santos et al., 2021; Zhu et al., 2021), whereas DOC species are released from biomass. While porewater exchange contributed to 60% of DIC and 36% of DOC outwelling, the DIC outwelling flux was 10-fold that of DOC. Our estimated DIC flux *via* porewater exchange and DIC outwelling were 1.2-fold and 3.2-fold of carbon burial, respectively. These results were similar to those of a recent investigation of Chongming Dongtan saltmarsh (Liu et al., 2021), where DIC export was 3-fold greater than local carbon burial. Overall, the carbon burial rate ($9.42\times10^5$ mol $d^{-1}$) accounted for 74% of the porewater-related carbon fluxes ($1.27\times10^6$ mol $d^{-1}$) and 28% of the carbon outwelling ($3.34\times10^6$ mol $d^{-1}$). Hence, porewater-derived carbon outwelling can be considered a mechanism for long-term carbon sink because bicarbonate (the dominant species in DIC) can remain in the ocean for 100,000 yr under a relatively stable pH circumstance (Santos et al., 2019; Middelburg et al., 2020; Xin et al., 2022; Yau et al., 2022).

Greenhouse gases were minor components of porewater-derived carbon fluxes compared with DIC fluxes (**Figure 8**). The $CO_2$ ($9.92\times10^4$ mol $d^{-1}$) and $CH_4$ ($6.06\times10^2$ mol $d^{-1}$) fluxes *via* porewater exchange contributed 75% and 100% of those fluxes in atmospheric evasion, respectively. Although the $CO_2$ and $CH_4$ fluxes were at least one order of magnitude lower than the carbon burial rate, their greenhouse effects cannot be ignored. Converting $CH_4$ fluxes into $CO_2$ equivalents by global warming potential values of 96 for emission time frames of 20 yr (Alvarez et al., 2018), and converting molar units to mass units. Here, the $CO_2$-equivalent greenhouse gas emissions would be 6.7 t $CO_2$-C $d^{-1}$, while total sediment carbon burial would be 41.4 t $CO_2$-C $d^{-1}$ in Andong Shoal. Therefore, porewater-derived greenhouse gas emissions may offset 16% of sediment carbon burial.

## 4 CONCLUSIONS

In this study, based on a spatial survey of porewater, surface water, sediment, and saltmarsh plants in a subtropical multi-species saltmarsh, we draw the following conclusions:

(1) The stable carbon isotope ($\delta^{13}C$) and C/N ratio suggest that the dominant C3 species *Scirpus mariqueter*, is the main

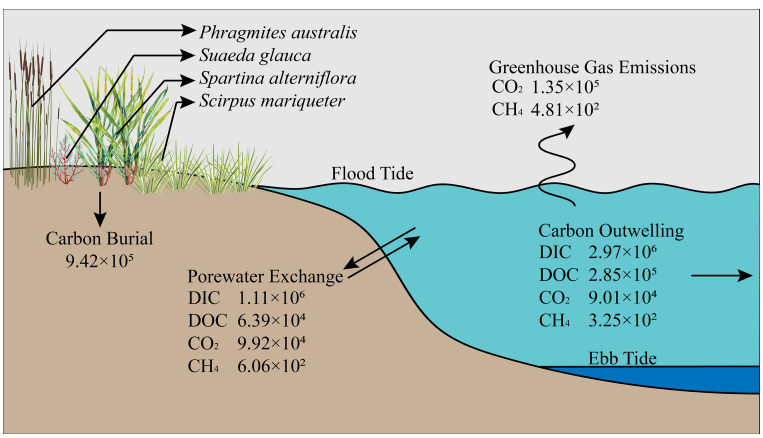


**FIGURE 8** | Conceptual model of major carbon flows (including carbon burial, porewater exchange, carbon outwelling and GHG emissions, mol $d^{-1}$) in Andong Shoal.

organic carbon source for the sediment and water column when study area is invaded by C4 species *Spartina alterniflora*.

(2) There was 5.60 ± 2.78 cm $d^{-1}$ of $^{222}$Rn-based porewater exchange rate, which implicated porewater-derived DIC, DOC $CO_2$ and $CH_4$ fluxes (mmol $m^{-2}$ $d^{-1}$) at 447 ± 227, 26 ± 20, 40 ± 21 and 0.25 ± 0.13, respectively. Porewater-derived DIC and DOC fluxes supported 60% and 36% of the corresponding species in carbon outwelling.

(3) Combining our results (porewater exchange, carbon outwelling, and greenhouse gas emissions) with literature data (i.e., carbon burial), porewater-derived DIC flux and DIC outwelling flux were 1.2-fold and 3.2-fold that of carbon burial, respectively. In addition to saltmarsh carbon burial, the DIC input to the ocean can be an important carbon sink because DIC can remain for a long duration.

(4) Although $CO_2$ and $CH_4$ were minor components in carbon pathways compared with DIC, their water-air emissions contributed by porewater carbon can offset 16% of the saltmarsh carbon sequester.

Overall, we highlight the importance of porewater exchange-related carbon outwelling as a long-term carbon sink in multi-species saltmarshes and the potential fate of atmospheric carbon fixed by saltmarsh vegetation. These provide a scientific basis for the protection and restoration of saltmarshes in the context of global climate change. The seasonal change and the organic carbon lability in saltmarshes deserve further studies because of their influence on quantification of blue carbon flux and evaluation of potential carbon sink.

## DATA AVAILABILITY STATEMENT

The original contributions presented in the study are included in the article/supplementary material. Further inquiries can be directed to the corresponding authors.

## AUTHOR CONTRIBUTIONS

PZ, XC, and LL designed the study; XC, YZ, QZ, XW, HZ, and LQ conducted the field work; PZ and XC performed the experiments and analyzed the data. PZ wrote the manuscript with contributions from all authors. All authors read and approved the final manuscript.

## FUNDING

This research was supported by the Zhejiang Provincial Natural Science Foundation of China (LQ21D060005), Natural Science Foundation of China (42006152) and China Postdoctoral Science Foundation (2020M681931).

## ACKNOWLEDGMENTS

We would like to thank Danping Huang for her kind assistance in the laboratory.

## REFERENCES

Alongi, D. M. (2020). Carbon Balance in Salt Marsh and Mangrove Ecosystems: A Global Synthesis. *J. Mar. Sci. Eng.* 8 (10), 767. doi: 10.3390/jmse8100767

Alvarez, R. A., Zavala-Araiza, D., Lyon, D. R., Allen, D. T., Barkley, Z. R., Brandt, A. R., et al. (2018). Assessment of Methane Emissions From the US Oil and Gas Supply Chain. *Science* 361 (6398), 186–188. doi: 10.1126/science.aar7204

Borges, A. V., Vanderborght, J. P., Schiettecatte, L. S., Gazeau, F. D. R., Ferrón-Smith, S., Delille, B., et al. (2004). Variability of the Gas Transfer Velocity of $CO_2$ in a Macrotidal Estuary (the Scheldt). *Estuaries* 27 (4), 593–603. doi: 10.1007/BF02907647

Burnett, W. C., and Dulaiova, H. (2003). Estimating the Dynamics of Groundwater Input Into the Coastal Zone *via* Continuous Radon-222 Measurements. *J. Environ. Radioact.* 69 (1-2), 21–35. doi: 10.1016/s0265-931x(03)00084-5

Cao, Y., Cao, Y., Li, G., Tian, Y., Fang, X., Li, Y., et al. (2020). Linking Ecosystem Services Trade-Offs, Bundles and Hotspot Identification With Cropland Management in the Coastal Hangzhou Bay Area of China. *Land. Use Policy* 97, 104689. doi: 10.1016/j.landusepol.2020.104689

Chen, X., Cukrov, N., Santos, I. R., Rodellas, V., Cukrov, N., and Du, J. (2020a). Karstic Submarine Groundwater Discharge Into the Mediterranean: Radon-Based Nutrient Fluxes in an Anchialine Cave and a Basin-Wide Upscaling. *Geochim. Cosmochimic. Acta* 268, 467–484. doi: 10.1016/j.gca.2019.08.019

Chen, X., Du, J., Yu, X., and Wang, X. (2021a). Porewater-Derived Dissolved Inorganic Carbon and Nutrient Fluxes in a Saltmarsh of the Changjiang River Estuary. *Acta Oceanol. Sin.* 40 (8), 32–43. doi: 10.1007/s13131-021-1797-z

Chen, X., Santos, I. R., Call, M., Reithmaier, G. M. S., Maher, D., Holloway, C., et al. (2021b). The Mangrove $CO_2$ Pump: Tidally Driven Pore-Water Exchange. *Limnol. Oceanog.* 66 (4), 1563–1577. doi: 10.1002/lno.11704

Chen, X., Santos, I. R., Hu, D., Zhan, L., Zhang, Y., Zhao, Z., et al. (2022). Porewater Exchange Flushes Blue Carbon From Intertidal Saltmarsh Sediments Into the Sea. *Limnol. Oceanog. Lett*. doi: 10.1002/lol2.10236

Chen, X., Ye, Q., Sanders, C. J., Du, J., and Zhang, J. (2020b). Bacterial-Derived Nutrient and Carbon Source-Sink Behaviors in a Sandy Beach Subterranean Estuary. *Mar. Pollut. Bull.* 160, 111570. doi: 10.1016/j.marpolbul.2020.111570

Chen, X., Zhang, F., Lao, Y., Wang, X., Du, J., and Santos, I. R. (2018). Submarine Groundwater Discharge-Derived Carbon Fluxes in Mangroves: An Important Component of Blue Carbon Budgets? *J. Geophy. Res.: Ocean.* 123 (9), 6962–6979. doi: 10.1029/2018jc014448

Chmura, G. L., and Aharon, P. (1995). Stable Carbon Isotope Signatures of Sedimentary Carbon in Coastal Wetlands as Indicators of Salinity Regime. *J. Coast. Res.* 11 (1), 124–135.

Chmura, G. L., Kellman, L., van Ardenne, L., and Guntenspergen, G. R. (2016). Greenhouse Gas Fluxes From Salt Marshes Exposed to Chronic Nutrient Enrichment. *PloS One* 11 (2), e0149937. doi: 10.1371/journal.pone.0149937

Chu, S. N., Wang, Z. A., Gonneea, M. E., Kroeger, K. D., and Ganju, N. K. (2018). Deciphering the Dynamics of Inorganic Carbon Export From Intertidal Salt Marshes Using High-Frequency Measurements. *Mar. Chem.* 206, 7–18. doi: 10.1016/j.marchem.2018.08.005

Corbett, D. R., Burnett, W. C., Cable, P. H., and Clark, S. B. (1998). A Multiple Approach to the Determination of Radon Fluxes From Sediments. *J. Radioanal. Nucl. Chem.* 236 (1-2), 247–252. doi: 10.1007/BF02386351

Correa, R. E., Xiao, K., Conrad, S. R., Wadnerkar, P. D., Wilson, A. M., Sanders, C. J., et al (2021). Groundwater Carbon Exports Exceed Sediment Carbon Burial in a Salt Marsh. *Estuar. Coast.* doi: 10.1007/s12237-021-01021-1

Czapla, K. M., Anderson, I. C., and Currin, C. A. (2020). Net Ecosystem Carbon Balance in a North Carolina, USA, Salt Marsh. *J. Geophy. Res.: Biogeosci.* 125 (10). doi: 10.1029/2019jg005509

Degens, E. T. (1969). "Biogeochemistry of Stable Carbon Isotopes," in *Organic Geochemistry*. Eds. G. Eglinton and M. T. J. Murphy (Berlin, Heidelberg: Springer), 304–329.

Duarte, C. M., Losada, I. J., Hendriks, I. E., Mazarrasa, I., and Marbà, N. (2013). The Role of Coastal Plant Communities for Climate Change Mitigation and Adaptation. *Nat. Climate Change* 3 (11), 961–968. doi: 10.1038/nclimate1970

Duarte, C. M., Middelburg, J., and Caraco, N. (2005). Major Role of Marine Vegetation on the Oceanic Carbon Cycle. *Biogeosciences* 2 (1), 1–8. doi: 10.5194/bg-2-1-2005

Gao, J., Bai, F., Yang, Y., Gao, S., Liu, Z., and Li, J. (2012). Influence of Spartina Colonization on the Supply and Accumulation of Organic Carbon in Tidal Salt Marshes of Northern Jiangsu Province, China. *J. Coast. Res.* 280, 486–498. doi: 10.2112/jcoastres-d-11-00062.1

Gao, S., Du, Y., Xie, W., Gao, W., Wang, D., and Wu, X. (2014). Environment-Ecosystem Dynamic Processes of Spartina Alterniflora Salt-Marshes Along the Eastern China Coastlines. *Sci. China Earth Sci.* 57 (11), 2567–2586. doi: 10.1007/s11430-014-4954-9

Garcia-Orellana, J., Rodellas, V., Tamborski, J., Diego-Feliu, M., Van Beek, P., Weinstein, Y., et al. (2021). Radium Isotopes as Submarine Groundwater Discharge (SGD) Tracers: Review and Recommendations. *Earth-Sc. Rev.* 220, 103681. doi: 10.1016/j.earscirev.2021.103681

Gatland, J. R., Santos, I. R., Maher, D. T., Duncan, T. M., and Erler, D. V. (2014). Carbon Dioxide and Methane Emissions From an Artificially Drained Coastal Wetland During a Flood: Implications for Wetland Global Warming Potential. *J. Geophy. Res.: Biogeosci.* 119 (8), 1698–1716. doi: 10.1002/2013jg002544

Guimond, J., and Tamborski, J. (2021). Salt Marsh Hydrogeology: A Review. *Water* 13 (4), 543. doi: 10.3390/w13040543

Herrmann, M., Najjar, R. G., Kemp, W. M., Alexander, R. B., Boyer, E. W., Cai, W.-J., et al. (2015). Net Ecosystem Production and Organic Carbon Balance of U.S. East Coast Estuaries: A Synthesis Approach. *Global Biogeochem. Cycle.* 29 (1), 96–111. doi: 10.1002/2013gb004736

He, T., Zhang, F., Wang, Y., Chen, X., and Du, J. (2022). Characterization of Dissolved Organic Matter in Submarine Groundwater From a Salt Marsh in Chongming Island, China. *J. Oceanol. Limnol.* 40, 128–141. doi: 10.1007/s00343-021-0296-6

Huang, S., Chen, Y. and , and Li, Y. (2020). Spatial Dynamic Patterns of Saltmarsh Vegetation in Southern Hangzhou Bay: Exotic and Native Species. *Water Sc. Eng.* 13 (1), 34–44. doi: 10.1016/j.wse.2020.03.003

Ho, D. T., Coffineau, N., Hickman, B., Chow, N., Koffman, T., and Schlosser, P. (2016). Influence of Current Velocity and Wind Speed on Air-Water Gas Exchange in a Mangrove Estuary. *Geophy. Res. Lett.* 43 (8), 3813–3821. doi: 10.1002/2016gl068727

Kroon, H. (1993). Determination of Nitrogen in Water: Comparison of a Continuous-Flow Method With on-Line UV Digestion With the Original Kjeldahl Method. *Anal. Chimica. Acta* 276 (2), 287–293. doi: 10.1016/0003-2670(93)80396-3

Liu, S. M., Hong, G. H., Zhang, J., Ye, X. W., and Jiang, X. L. (2009). Nutrient Budgets for Large Chinese Estuaries. *Biogeosciences* 6, 2245–2263. doi: 10.5194/bg-6-2245-2009

Liu, J., Yu, X., Chen, X., Du, J., and Zhang, F. (2021). Utility of Radium Quartet for Evaluating Porewater-Derived Carbon to a Saltmarsh Nearshore Water: Implications for Blue Carbon Export. *Sci. Tot. Environ.* 764, 144238. doi: 10.1016/j.scitotenv.2020.144238

Liu, L., Zhou, J., Zheng, B., Cai, W., Lin, K., and Tang, J. (2013). Temporal and Spatial Distribution of Red Tide Outbreaks in the Yangtze River Estuary and Adjacent Waters, China. *Mar. Pollut. Bull.* 72, 213–221. doi: 10.1016/j.marpolbul.2013.04.002

Li, Y., and Xie, Q. (1993). Zonation of Sediment and Sedimentary Rate on Andong Tidal Flat in Hangzhou Bay, China. *Donghai. Mar. Sci.* 11 (1), 21–33.

Lo Iacono, C., Mateo, M. A., Gràcia, E., Guasch, L., Carbonell, R., Serrano, L., et al. (2008). Very High-Resolution Seismo-Acoustic Imaging of Seagrass Meadows (Mediterranean Sea): Implications for Carbon Sink Estimates. *Geophy. Res. Lett.* 35 (18). doi: 10.1029/2008gl034773

McLeod, E., Chmura, G. L., Bouillon, S., Salm, R., Björk, M., Duarte, C. M., et al. (2011). A Blueprint for Blue Carbon: Toward an Improved Understanding of the Role of Vegetated Coastal Habitats in Sequestering $CO_2$. *Front. Ecol. Environ.* 9 (10), 552–560. doi: 10.1890/110004

Meyers, P. A. (1994). Preservation of Elemental and Isotopic Source Identification of Sedimentary Organic Matter. *Chem. Geology.* 114 (3-4), 289–302. doi: 10.1016/0009-2541(94)90059-0

Middelburg, J. J., Soetaert, K., and Hagens, M. (2020). Ocean Alkalinity, Buffering and Biogeochemical Processes. *Rev. Geophys.* 58 (3), e2019RG000681. doi: 10.1029/2019RG000681

Moore, W. S., and Arnold, R. (1996). Measurement of $^{223}$Ra and $^{224}$Ra in Coastal Waters Using a Delayed Coincidence Counter. *J. Geophy. Res.: Ocean.* 101 (C1), 1321–1329. doi: 10.1029/95jc03139

Najjar, R. G., Herrmann, M., Alexander, R., Boyer, E. W., Burdige, D. J., Butman, D., et al. (2018). Carbon Budget of Tidal Wetlands, Estuaries, and Shelf Waters of Eastern North America. *Global Biogeochem. Cycle.* 32 (3), 389–416. doi: 10.1002/2017gb005790

Neubauer, S. C., and Anderson, I. C. (2003). Transport of Dissolved Inorganic Carbon From a Tidal Freshwater Marsh to the York River Estuary. *Limnol. Oceanog.* 48 (1), 299–307. doi: 10.4319/lo.2003.48.1.0299

Pérez, A., Machado, W., Gutierrez, D., Smoak, J. M., Breithaupt, J. L., Saldarriaga, M. S., et al. (2020). Carbon and Nutrient Accumulation in Mangrove Sediments Affected by Multiple Environmental Changes. *J. Soils. Sediment.* 20 (5), 2504–2509. doi: 10.1007/s11368-020-02612-4

Peterson, R. N., Burnett, W. C., Dimova, N., and Santos, I. R. (2009). Comparison of Measurement Methods for Radium-226 on Manganese-Fiber. *Limnol. Oceanog.: Methods* 7, 196–205. doi: 10.4319/lom.2009.7.196

Reithmaier, G. M., Johnston, S. G., Junginger, T., Goddard, M. M., Sanders, C. J., Hutley, L. B., et al. (2021). Alkalinity Production Coupled to Pyrite Formation Represents an Unaccounted Blue Carbon Sink. *Glob. Biogeochem. Cycle* 35 (4), e2020GB006785. doi: 10.1029/2020GB006785

Rosentreter, J. A., Maher, D. T., Ho, D. T., Call, M., Barr, J. G., and Eyre, B. D. (2017). Spatial and Temporal Variability of $CO_2$ and $CH_4$ Gas Transfer Velocities and Quantification of the CH4 Microbubble Flux in Mangrove Dominated Estuaries. *Limnol. Oceanog.* 62 (2), 561–578. doi: 10.1002/lno.10444

Santos, I. R., Burdige, D. J., Jennerjahn, T. C., Bouillon, S., Cabral, A., Serrano, O., et al. (2021). The Renaissance of Odum's Outwelling Hypothesis in 'Blue Carbon' Science. *Estuar. Coast. Shelf. Sci.* 255, 107361. doi: 10.1016/j.ecss.2021.107361

Santos, I. R., Chen, X., Lecher, A. L., Sawyer, A. H., Moosdorf, N., Rodellas, ,. V., et al. (2021b). Submarine Groundwater Discharge Impacts on Coastal Nutrient Biogeochemistry. *Nat. Rev. Earth Environ.* 2, 307–323. doi: 10.1038/s43017-021-00152-0

Santos, I. R., Maher, D. T., and Eyre, B. D. (2012). Coupling Automated Radon and Carbon Dioxide Measurements in Coastal Waters. *Environ. Sci. Technol.* 46 (14), 7685–7691. doi: 10.1021/es301961b

Santos, I. R., Maher, D. T., Larkin, R., Webb, J. R., and Sanders, C. J. (2019). Carbon Outwelling and Outgassing vs. Burial in an Estuarine Tidal Creek Surrounded by Mangrove and Saltmarsh Wetlands. *Limnol. Oceanog.* 64 (3), 996–1013. doi: 10.1002/lno.11090

Seyfferth, A. L., Bothfeld, F., Vargas, R., Stuckey, J. W., Wang, J., Kearns, K., et al. (2020). Spatial and Temporal Heterogeneity of Geochemical Controls on Carbon Cycling in a Tidal Salt Marsh. *Geochim. Cosmochimic. Acta* 282, 1–18. doi: 10.1016/j.gca.2020.05.013

Song, H., Yu, H., Wang, H., Fan, D., Hu, B., and Wang, F. (2014). Biogenic Traces in Modern Shoal Deposits of Andong Area, Hangzhou Bay. *J. Palaeogeogr. (Chinese. Edition).* 16 (5), 703–714. doi: 10.7605/gdlxb.2014.05.56

Taillardat, P., Willemsen, P., Marchand, C., Friess, D. A., Widory, D., Baudron, P., et al. (2018). Assessing the Contribution of Porewater Discharge in Carbon Export and $CO_2$ Evasion in a Mangrove Tidal Creek (Can Gio, Vietnam). *J. Hydrol.* 563, 303–318. doi: 10.1016/j.jhydrol.2018.05.042

Tait, D. R., Maher, D. T., Macklin, P. A., and Santos, I. R. (2016). Mangrove Pore Water Exchange Across a Latitudinal Gradient. *Geophy. Res. Lett.* 43 (7), 3334–3341. doi: 10.1002/2016GL068289

Tamborski, J. J., Eagle, M., Kurylyk, B. L., Kroeger, K. D., Wang, Z. A., Henderson, P., et al. (2021). Pore Water Exchange-Driven Inorganic Carbon Export from Intertidal Salt Marshes. *Limnol. Oceanogr.* 66 (5), 1774–1792. doi: 10.1002/lno.11721

Tang, J., Ye, S., Chen, X., Yang, H., Sun, X., Wang, F., et al. (2018). Coastal Blue Carbon: Concept, Study Method, and the Application to Ecological Restoration. *Sci. China Earth Sci.* 61 (6), 637–646. doi: 10.1007/s11430-017-9181-x

Taniguchi, M., Dulai, H., Burnett, K. M., Santos, I. R., Sugimoto, R., Stieglitz, T., et al. (2019). Submarine Groundwater Discharge: Updates on Its Measurement Techniques, Geophysical Drivers, Magnitudes, and Effects. *Front. Environ. Sci.* 7. doi: 10.3389/fenvs.2019.00141

Wang, Z. A., and Cai, W. J. (2004). Carbon Dioxide Degassing and Inorganic Carbon Export From a Marsh-Dominated Estuary (the Duplin River): A Marsh $CO_2$ Pump. *Limnol. Oceanog.* 49 (2), 341–354. doi: 10.4319/lo.2004.49.2.0341

Wang, Z. A., Kroeger, K. D., Ganju, N. K., Gonneea, M. E., and Chu, S. N. (2016). Intertidal Salt Marshes as an Important Source of Inorganic Carbon to the Coastal Ocean. *Limnol. Oceanog.* 61 (5), 1916–1931. doi: 10.1002/lno.10347

Wang, X. C., and Lee, C. (1994). Sources and Distribution of Aliphatic Amines in Salt Marsh Sediment. *Organ. Geochem.* 22 (6), 1005–1021. doi: 10.1016/0146-6380(94)90034-5Get

Wang, F., Sanders, C. J., Santos, I. R., Tang, J., Schuerch, M., Kirwan, M. L., et al. (2021). Global Blue Carbon Accumulation in Tidal Wetlands Increases With Climate Change. *Natl. Sci. Rev* 8 (9), nwaa296. doi: 10.1093/nsr/nwaa296

Wang, F., Xiao, K., Santos, I. R., Lu, Z., Tamborski, J., Wang, Y., et al. (2022). Porewater Exchange Drives Nutrient Cycling and Export in a Mangrove-Salt Marsh Ecotone. *J. Hydrol.* 606, 127401. doi: 10.1016/j.jhydrol.2021.127401

Wang, D., Zhang, R., Xiong, J., Guo, H.-Q., and Zhao, B. (2015). Contribution of Invasive Species Spartina Alterniflora to Soil Organic Carbon Pool in Coastal Wetland: Stable Isotope Approach. *Chin. J. Plant Ecol.* 39 (10), 941–949. doi: 10.17521/cjpe.2015.0091. a.

Wanninkhof, R. (2014). Relationship Between Wind Speed and Gas Exchange Over the Ocean Revisited. *Limnol. Oceanog.: Methods* 12 (6), 351–362. doi: 10.4319/lom.2014.12.351

Wu, T., Wu, M., and Xiao, J. (2008). Dynamics of Community Succession and Species Diversity of Vegetations in Beach Wetlands of Hangzhou Bay. *Chinese. J. Ecol.* 27 (8), 1284–1289. doi: 10.13292/j.1000

Wu, Z., Zhu, H., Tang, D., Wang, Y., Zidan, A., and Cui, Z. (2021). Submarine Groundwater Discharge as a Significant Export of Dissolved Inorganic Carbon From a Mangrove Tidal Creek to Qinglan Bay (Hainan Island, China). *Continent. Shelf. Res.* 223, 104451. doi: 10.1016/j.csr.2021.104451

Xia, T., Chen, Y., Gao, J., and Huang, S. (2019). Impact of Vegetation Succession on Salt Marsh Material Circulation in Southern Hangzhou Bay. *Mar. Sci.* 43 (10), 35–42. doi: 10.11759/hykx20190224001

Xiao, K., Wilson, A. M., Li, H., Santos, I. R., Tamborski, J., Smith, E., et al. (2020). Large $CO_2$ Release and Tidal Flushing in Salt Marsh Crab Burrows Reduce the Potential for Blue Carbon Sequestration. *Limnol. Oceanog.* 66 (1), 14–29. doi: 10.1002/lno.11582

Xin, P., Jin, G., Li, L., and Barry, D. A. (2009). Effects of Crab Burrows on Pore Water Flows in Salt Marshes. *Adv. Water Resour.* 32 (3), 439–449. doi: 10.1016/j.advwatres.2008.12.008

Xin, P., Wilson, A., Shen, C., Ge, Z., Moffett, K. B., Santos, I. R., et al. (2022). Surface Water and Groundwater Interactions in Salt Marshes and Their Impact on Plant Ecology and Coastal Biogeochemistry. *Rev. Geophys.* 60 (1), e2021RG000740. doi: 10.1029/2021rg000740

Yau, Y. Y., Xin, P., Chen, X., Zhan, L., Call, M., Conrad, S., et al. (2022). Alkalinity Export to the Ocean Is a Major Carbon Sequestration Mechanism in a Macrotidal Saltmarsh. *Limnol. Oceanog.*

Young, M. E. G. a. N., Gonneea, M. E., Herrera-Silveira, J. O. R. G. E., and Paytan, A. D. I. N. A. (2005). Export of Dissolved and Particulate Carbon and Nitrogen From a Mangrove-Dominated Lagoon, Yucatan Peninsula, Mexico. *Int. J. Ecol. Environ. Sci.* 31, 189–202.

Yuan, J., Liu, D., Ji, Y., Xiang, J., Lin, Y., Wu, M., et al. (2019). Spartina Alterniflorainvasion Drastically Increases Methane Production Potential by Shifting Methanogenesis From Hydrogenotrophic to Methylotrophic Pathway in a Coastal Marsh. *J. Ecol.* 107 (5), 2436–2450. doi: 10.1111/1365-2745.13164

Zhu, Q., Cochran, J. K., Heilbrun, C., Yin, H., Feng, H., Tamborski, J. J., et al. (2021). Small-Scale Geochemical Heterogeneities and Seasonal Variation of Iron and Sulfide in Salt Marshes Revealed by Two-Dimensional Sensors. *Front. Earth Sci.* 9. doi: 10.3389/feart.2021.653698

**Conflict of Interest:** The authors declare that the research was conducted in the absence of any commercial or financial relationships that could be construed as a potential conflict of interest.

**Publisher's Note:** All claims expressed in this article are solely those of the authors and do not necessarily represent those of their affiliated organizations, or those of the publisher, the editors and the reviewers. Any product that may be evaluated in this article, or claim that may be made by its manufacturer, is not guaranteed or endorsed by the publisher.

**Citation:** *Zhu P, Chen X, Zhang Y, Zhang Q, Wu X, Zhao H, Qi L, Shao X and Li L (2022) Porewater-Derived Blue Carbon Outwelling and Greenhouse Gas Emissions in a Subtropical Multi-Species Saltmarsh.*
*Front. Mar. Sci. 9:884951. doi: 10.3389/fmars.2022.884951*